IOP Publishing
Nanotechnology
Nanotechnology 25 (2014) 155201 (7pp) doi:10.1088/0957-4484/25/15/155201

Gate-bias stress-dependent photoconductive characteristics of multi-layer MoS_2 field-effect transistors

Kyungjune Cho[1], Tae-Young Kim[1], Woanseo Park[1], Juhun Park[1], Dongku Kim[1], Jingon Jang[1], Hyunhak Jeong[1], Seunghun Hong[1,2] and Takhee Lee[1]

[1] Department of Physics and Astronomy, and Institute of Applied Physics, Seoul National University, Seoul 151-747, Korea
[2] Department of Biophysics and Chemical Biology, Seoul National University, Seoul 151-747, Korea

E-mail: tlee@snu.ac.kr

Received 21 November 2013, revised 8 February 2014
Accepted for publication 19 February 2014
Published 18 March 2014

Abstract
We investigated the photoconductive characteristics of molybdenum disulfide (MoS_2) field-effect transistors (FETs) that were fabricated with mechanically exfoliated multi-layer MoS_2 flakes. Upon exposure to UV light, we observed an increase in the MoS_2 FET current because of electron–hole pair generation. The MoS_2 FET current decayed after the UV light was turned off. The current decay processes were fitted using exponential functions with different decay characteristics. Specifically, a fast decay was used at the early stages immediately after turning off the light to account for the exciton relaxation, and a slow decay was used at later stages long after turning off the light due to charge trapping at the oxygen-related defect sites on the MoS_2 surface. This photocurrent decay phenomenon of the MoS_2 FET was influenced by the measurement environment (i.e., vacuum or oxygen environment) and the electrical gate-bias stress conditions (positive or negative gate biases). The results of this study will enhance the understanding of the influence of environmental and measurement conditions on the optical and electrical properties of MoS_2 FETs.

Keywords: molybdenum disulfide, field-effect transistors, photoresponse

(Some figures may appear in colour only in the online journal)

1. Introduction

Two-dimensional (2D) nanomaterials, such as graphene, have garnered great attention for their usage in ultrathin layered device structures [1, 2]. Graphene has several advantages, such as a high charge mobility, transparency, mechanical strength, and flexibility [3–5], that make it well suited for 2D atomic-layer electronic device applications. However, the use of graphene as a semiconductor is limited because of the absence of an energy band gap. At best, a narrow band gap with a sacrifice of mobility allows the fabrication of graphene nanoribbons [6].

Unlike graphene, dichalcogenide layered materials, such as MoS_2, $MoSe_2$, and WSe_2, have attracted significant interest because of their band gap semiconducting properties. For example, molybdenum disulfide (MoS_2) has an indirect band gap of 1.2 eV as a bulk material and a direct band gap of 1.8 eV as a single layer [7, 8]. Furthermore, it has been reported that the single-layer MoS_2 field-effect transistor (FET) has a high carrier mobility of $\sim$200 $cm^2\ V^{-1}\ s^{-1}$ with a high-k dielectric layer, such as HfO_2 [2]. MoS_2 has other excellent features, such as mechanical flexibility, optical sensitivity, and photoconductivity [9–12], that allow the use of MoS_2 nanosheets in transistors, phototransistors, sensors, and memory and logic circuits [13–20]. Recently, Yin *et al* fabricated single-layer MoS_2 phototransistors and investigated the photoresponsivity at different illuminated optical powers [21]. Lee *et al* also

 © 2014 IOP Publishing Ltd Printed in the UK

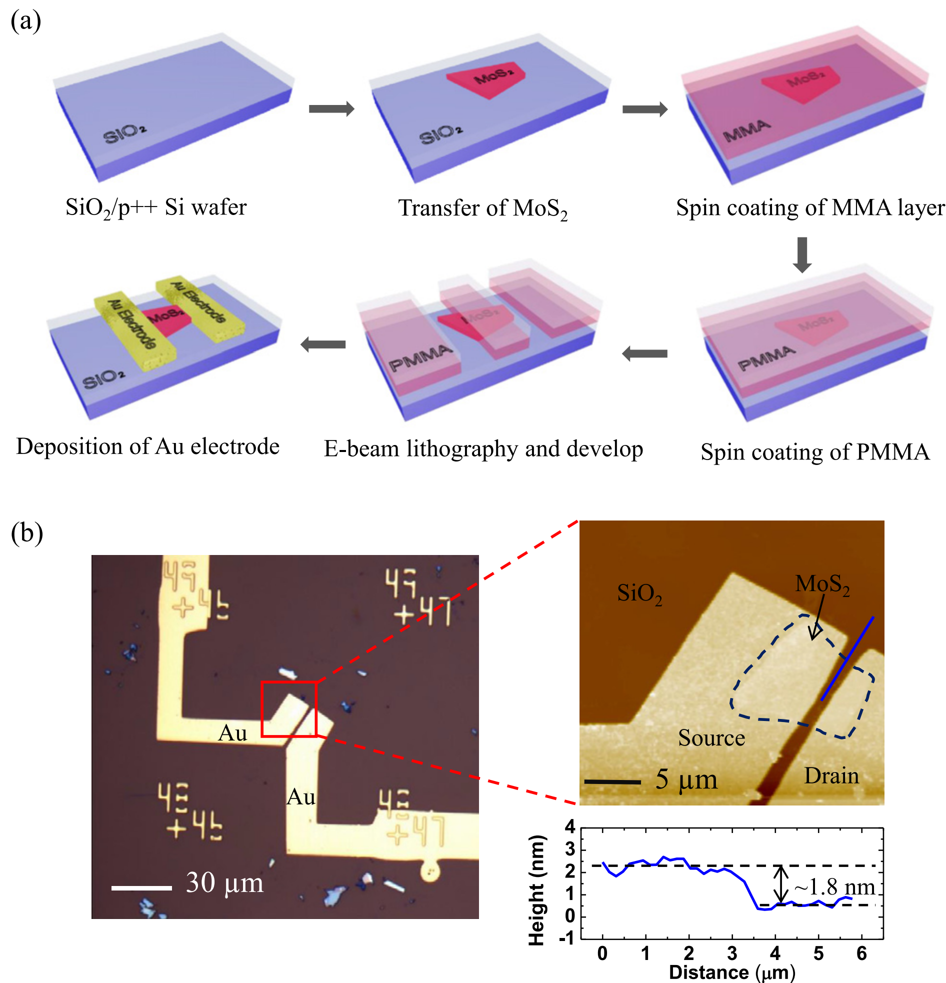

Figure 1. (a) Schematics illustrating the device fabrication procedures. (b) Optical image of the MoS_2 FET device (left), AFM image of the device (right top) and topological cross-sectional profile across a blue line in the AFM image (right bottom) indicating the three layers of the MoS_2 flake.

studied MoS_2 phototransistors and reported the optical energy gap of MoS_2 as a function of the MoS_2 film layer thickness [22]. Interestingly, the properties of MoS_2 FETs are influenced by the oxygen environment, chemical adsorptions of oxygen and water molecules and electrical-induced stresses. Several groups, including ours, have reported that a significant variation in the transport characteristics of MoS_2 FETs occurs due to these extrinsic environmental or measurement effects. This variation complicates the investigation of the intrinsic properties of MoS_2 FETs [23–27], such as photoconductivity, which could be less than optimal. However, the photoconductive properties under various environmental and measurement conditions have not been thoroughly investigated.

In the present study, we investigated the photoconductive characteristics of a multi-layer MoS_2 nanosheet under various oxygen environments and different electrical measurement conditions. The phototransistors were fabricated with MoS_2 sheets that were mechanically exfoliated from a bulk MoS_2 material, and their photocurrents were examined under various conditions with UV illumination. We analyzed the photocurrents of the MoS_2 FET device under different oxygen environments and gate-bias stress conditions in the presence and absence of UV light.

2. Experimental details

Figure 1(a) shows the schematic processes of the device fabrication for MoS_2 FETs. First, we prepared the Si wafer, which had a 270 nm thick SiO_2 layer. The Si wafer was heavily p^{++} doped (resistivity of $\sim 5 \times 10^{-3}$ Ω cm) and was used as a back gate. Second, MoS_2 flakes were transferred using the mechanical exfoliation method from a bulk MoS_2 crystal (purchased from SPI supplies) onto a Si wafer piece. Next, we identified the location of suitable MoS_2 flakes that were not too thick using an optical microscope. To verify the thickness of a MoS_2 flake, we measured its height using an atomic force microscope (AFM) (Park Systems, NX10). Figure 1(b) shows an optical image and an AFM image of a real device used in this study. From the AFM image, we measured the thickness of this particular MoS_2 flake to be 1.8 nm, which corresponds to the MoS_2 tri-layers. Next, to make patterns for the source and drain electrodes, we spin-coated a double-layer resist to act as the electron-beam resist using methyl methacrylate (MMA)

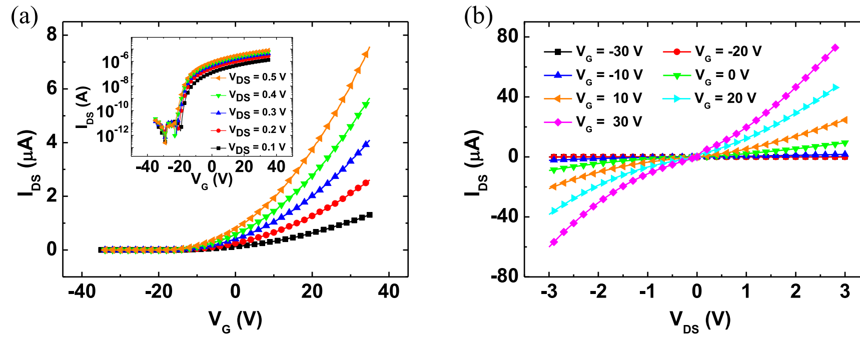

Figure 2. (a) I_{DS}–V_G curves measured with varying V_{DS} from 0.1 to 0.5 V. (b) I_{DS}–V_{DS} curves measured with varying V_G from −30 to 30 V.

(8.5%), MAA (9% concentration in ethyl lactate) and poly methyl methacrylate (PMMA) 950 K (5% concentration in anisole). We used this double-layer resist method to obtain fine electrode patterns. Next, we created windows in the resist layers, which would be defined as the source and drain electrodes, using an electron-beam lithography system (JEOL, JSM-6510) and development process. The electrodes were prepared by depositing Au (50-nm thick) on Ti (5-nm thick) using an electron-beam evaporator. After the MoS_2 FET device was fabricated, its electrical characteristics were measured using a semiconductor parameter analyzer (Keithley, 4200-SCS) in a probe station (Janis, ST-500) that allowed controlled environments, such as vacuum or variable oxygen pressures. To investigate the photoconductive properties of the fabricated device, we measured the source–drain current of the device while it was exposed to UV light (254 nm wavelength) using a UV illuminator.

3. Results and discussion

First, we measured the basic electrical characteristics of the MoS_2 FET device under vacuum conditions ($\sim 3.3 \times 10^{-4}$ Torr). Figure 2(a) displays the transfer characteristics (source–drain current versus gate voltage, I_{DS}–V_G) measured by varying the source–drain voltage from 0.1 to 0.5 V with an increment of 0.1 V. The inset of figure 2(a) shows the transfer characteristics on a semi-logarithmic scale. Figure 2(b) displays the output characteristics (source–drain current versus source–drain voltage, I_{DS}–V_{DS}) measured by varying the gate bias from −30 to 30 V with an increment of 10 V. The performance of the device may be affected by the back-gate-bias stress. However, the data of figure 2 was measured in vacuum conditions with a very short time period. For this reason, we can neglect the effect from gate-bias stress. The MoS_2 FET device exhibited n-channel FET behavior because a positive gate bias increased the source–drain current. From the transfer characteristics (figure 2(a)), the subthreshold swing (SS) value was observed as ∼1.43 V/dec. Also, the field-effect mobility (μ) was found to be ~ 1.6 cm^2 V^{-1} s^{-1} using the following formula, $\mu = [dI_{DS}/dV_G] \times [L/(WC_iV_{DS})]$, where the dI_{DS}/dV_G is the slope of the linear region (near V_G of ∼30 V) of the transfer curve, the channel length $(L) = 0.8$ μm, the channel width $(W) = 7$ μm, and the gate capacitance per area$(C_i) = \sim 1.3 \times 10^{-4}$ F m^{-2}. The gate capacitance refers to the capacitance between the MoS_2 active layer and the back gate per unit area (i.e., $C_i = \varepsilon_o \varepsilon_r / d$, where ε_o is the vacuum permittivity (8.85×10^{-12} F m^{-1}), ε_r is the dielectric constant of SiO_2 (∼3.9), and d is the SiO_2 layer's thickness (270 nm)). Note that we previously observed a hysteresis effect in the transfer characteristics for the double V_G sweep loop when measured in ambient conditions [23]. The hysteresis effect became more obvious at the slower V_G sweep rates and at the wider V_G sweep range, however the hysteresis effect was less obvious when the devices were measured in vacuum [23].

To investigate the photoconductive characteristics of the MoS_2 FET device, we measured the source–drain currents in the presence and absence of UV light. Figure 3 displays the photoresponsive characteristics of the MoS_2 FET device at a fixed source–drain voltage of 0.1 V under different environments (vacuum or oxygen environments). The photocurrent in figure 3(a) was measured under vacuum conditions of $\sim 3.3 \times 10^{-4}$ Torr. We previously reported that the gate bias could affect the electrical characteristics of MoS_2 FET devices [23]. Therefore, to eliminate such gate-bias stress effects, we applied 0 V to the gate of our device while measuring the photocurrents. The purple, boxed regions in figure 3 indicate the period when the UV illuminator was turned on. The current increased when the UV illuminator was turned on and decreased after the UV illuminator was turned off.

The data in figures 3(b)–(d) were obtained under the same bias conditions that were used to obtain the data in figure 3(a) but under different oxygen environments (oxygen pressures at 1.4 Torr, 0.98×10^1 Torr, and 2.2×10^2 Torr, respectively). The insets in figure 3 display the logarithmic scale plots of the currents, which were measured after the UV light was turned off. When we exposed the device to UV light, the UV light generated charge carriers in the MoS_2 layer and increased the source–drain current. After we turned off the UV light, the current started to decrease. This photocurrent phenomenon has been observed in various types of materials and devices, such as phototransistors made with ZnO nanowire, polycrystalline ZnO thin films, CdS nanoribbons, and WO_3 thin films, among others [28–32]. The increase in current upon exposure to UV light can be attributed to electron–hole pair generation, which occurs when the energy of the light is larger than the band gap of the material. In our case, the band gap of the tri-layer

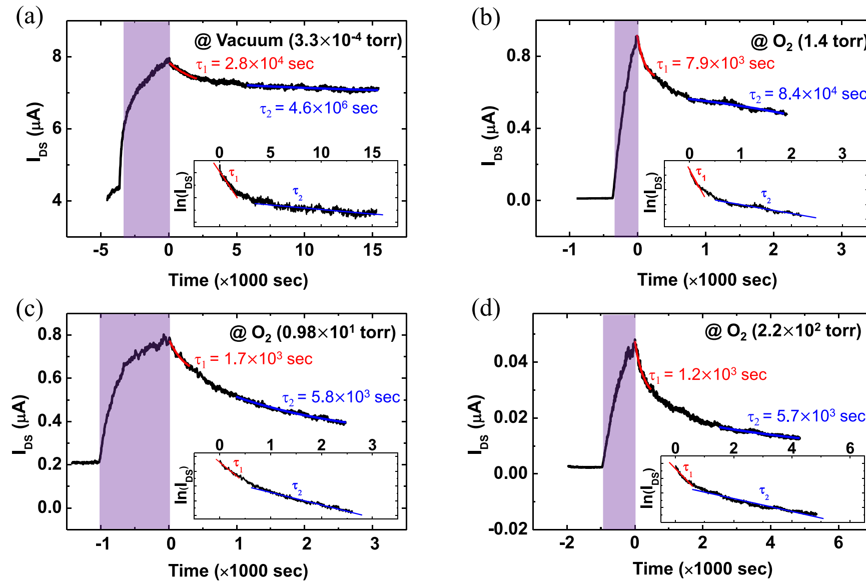

Figure 3. Photocurrent (I_{DS}) versus time characteristics measured at $V_{DS} = 0.1$ V and $V_G = 0$ V with and without UV illumination under (a) vacuum, and (b) oxygen pressure of 1.4 Torr, (c) 0.98×10^1 Torr, and (d) 2.2×10^2 Torr. Inset plots represent the logarithmic scale of photocurrent data after the turn-off of the UV light. Red and blue curves are exponential fitting curves with decay time constants (τ_1 or τ_2).

MoS_2 sheet is ~1.4 eV (approximately between 1.2 eV for bulk MoS_2 and 1.8 eV for single-layer MoS_2) [22].

The decay of currents after the UV light is turned off is often fitted with an exponential curve with a characteristic decay time constant. In our study, the photocurrent data could not be fitted with a single decay time constant. Therefore, our data were fitted with different exponential curves. In figure 3, we added two exponential fitting curves in two regimes: 'early stage' immediately after the turn-off of the UV light, and 'late stage' long after the turn-off of the UV light. These two stages were somewhat arbitrarily defined (see insets in figure 3). The data segments of the early and late stages (figure 3) were fitted with different decay time constants, τ_1 and τ_2, respectively. The τ_1 and τ_2 values were of the order of 10^3 s or longer (figure 3). Several studies have shown that the decay time constant ranges from tens of milliseconds to hours depending on the material type, device structure, and environment and measurement conditions [28–32]. Specifically, we observed that τ_1 was smaller than τ_2, which means that current at the early stages decreased rapidly compared with the later stages. This distinct decay phenomenon was also reported in various semiconductor materials, such as zinc oxide, cadmium sulfide, and tungsten oxide, among others [28–32]. In these materials, the distinct decay phenomenon occurred due to several reasons. For example, it was reported that in polycrystalline ZnO thin film transistors, the different types of adsorption of oxygen (for example, physical adsorption and chemical adsorption of oxygen) on the ZnO surface resulted in different trapping rates and therefore caused different decay processes [28]. In CdS nanoribbon FETs, the non-uniform thickness of the CdS layers caused different decay rates (i.e., a faster decay from thinner layers and a slower decay from thicker layers) [29]. The different decay processes in our study (i.e., fast decay at the early stages and slow decay at the late stages) could be attributed to exciton relaxation and charge trapping at the surface defect sites of MoS_2 or the recombination of captured electrons at the defect sites. Generally, exciton relaxation (i.e., electron–hole recombination) is a dominant mechanism at the early stage and is a fast decay in the form of an exponential function with a decay time constant [28–32]. In contrast, the charge trapping at the surface defect sites (such as the electron trapping of adsorbed oxygen molecules on the surface $[O_2 + e^- \rightarrow O_2^-]$) and the recombination of captured electrons at the surface defect sites (such as the recombination process $[O_2^- + h \rightarrow O_2]$) are dominant at the later stages with a slower decay time constant. All of these mechanisms lead to a decrease in the concentration of electrons that are generated by the UV illuminator, resulting in a current decay as shown in figure 3.

We investigated the photoconductive characteristics of the device under different oxygen pressures, as shown in figures 3(b)–(d). These data demonstrated similarities with the data measured under vacuum conditions (figure 3(a)). In addition, these data demonstrated that both the τ_1 and τ_2 values decreased with an increase in oxygen pressure. Specifically, the τ_1 and τ_2 values in vacuum were 2.8×10^4 s and 4.6×10^6 s, respectively. In addition, for an increase in oxygen pressure from 1.4 to 2.2×10^2 Torr, τ_1 decreased from 7.9×10^3 to 1.2×10^3 s and τ_2 decreased from 8.4×10^4 to 5.7×10^3 s. This phenomenon can be explained by electron trapping at the oxygen-related defect sites on the MoS_2 surface. As mentioned earlier, electrons can be trapped at the oxygen trap sites on the surface of MoS_2. This charge trapping leads to a decrease in current and hence smaller τ values for increasing oxygen pressures, as observed in figure 3. Note that the current level of the initial state of each measurement was different (figure 3). When we measured the photoresponse characteristics, we waited for several hours or even a day before

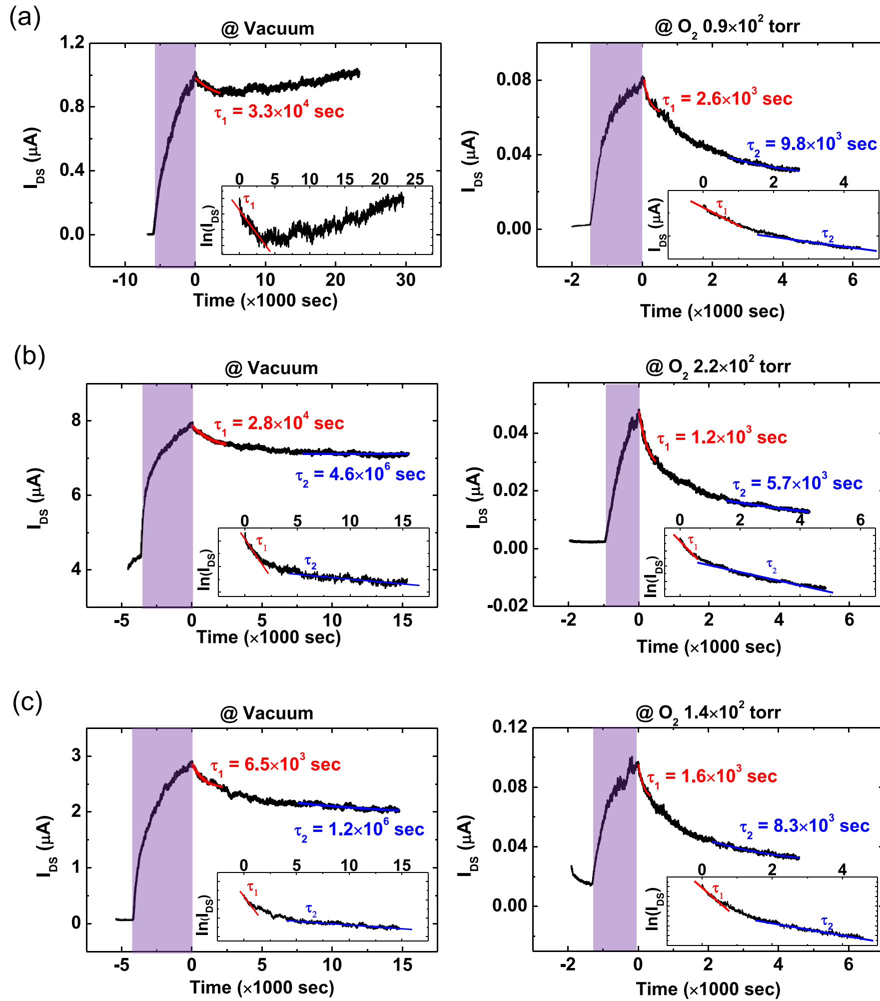

Figure 4. Photocurrent (I_{DS}) versus time characteristics measured at $V_{DS} = 0.1$ V with and without UV illumination when (a) a negative-gate-bias stress ($V_G = -20$ V) was applied, (b) no gate-bias stress ($V_G = 0$ V) was applied, and (c) a positive-gate-bias stress ($V_G = 20$ V) was applied. Plots in the left panel were measured in vacuum and plots in the right panel were measured in an oxygen environment. Inset plots represent the logarithmic scale of photocurrent data after the turn-off of the UV light.

each measurement to make the device recover from the UV illumination effect. However, in some cases the device did not fully recover, thus the current level of the initial state of each measurement was different. Also note that the UV illumination time was not the same in each measurement (figure 3). While we monitored the current during UV illumination, the current quickly increased initially and then slowed down and became saturated. We waited long enough for the current to become saturated, but this process was different among the measurement cases. During the measurements, after the current appeared to become sufficiently saturated (the zoomed-in data region is not provided here), we turned off the UV light. For this reason, the UV illumination time was not the same among the measurement cases.

The photocurrent gradually increased and decreased in our study (figure 3). Some observed fast photocurrent change [21] while others observed gradual change [26] in MoS_2 FET devices. Similar gradual photocurrent change was also observed in other types of semiconducting devices. For example, in the case of the ZnO nanowire FET, the extent of photocurrent increase sensitively depended on the measurement environment; the photocurrent rise was fast in the air environment and it was gradual in vacuum [31].

In our previous study, we reported that the MoS_2 FET devices are affected by the gate-bias electrical stress [23]. Specifically, the electrical properties of MoS_2 FETs could be significantly affected by the electrical gate-bias stress type, sweep rate, and duration. For example, when a positive-gate-bias stress was applied to the MoS_2 FET, the current of the device decreased and its threshold shifted in the positive-gate-bias direction. In contrast, for a negative-gate-bias stress, the current of the device increased and the threshold shifted in the negative-gate-bias direction [23]. Therefore, to investigate the photoconductive responses of the device under gate-bias stress, we measured the photocurrents from the device by applying positive or negative gate bias under vacuum conditions. Figures 4(a)–(c) show the photoresponses of the device measured with an applied gate voltage of −20 V, 0, and +20 V with the same bias condition ($V_{DS} = 0.1$ V), respectively, in vacuum (left panel of figure 4) and oxygen environments (right panel of figure 4) The photocurrent response to gate-bias stress is similar to that to zero gate bias. However, the current decay

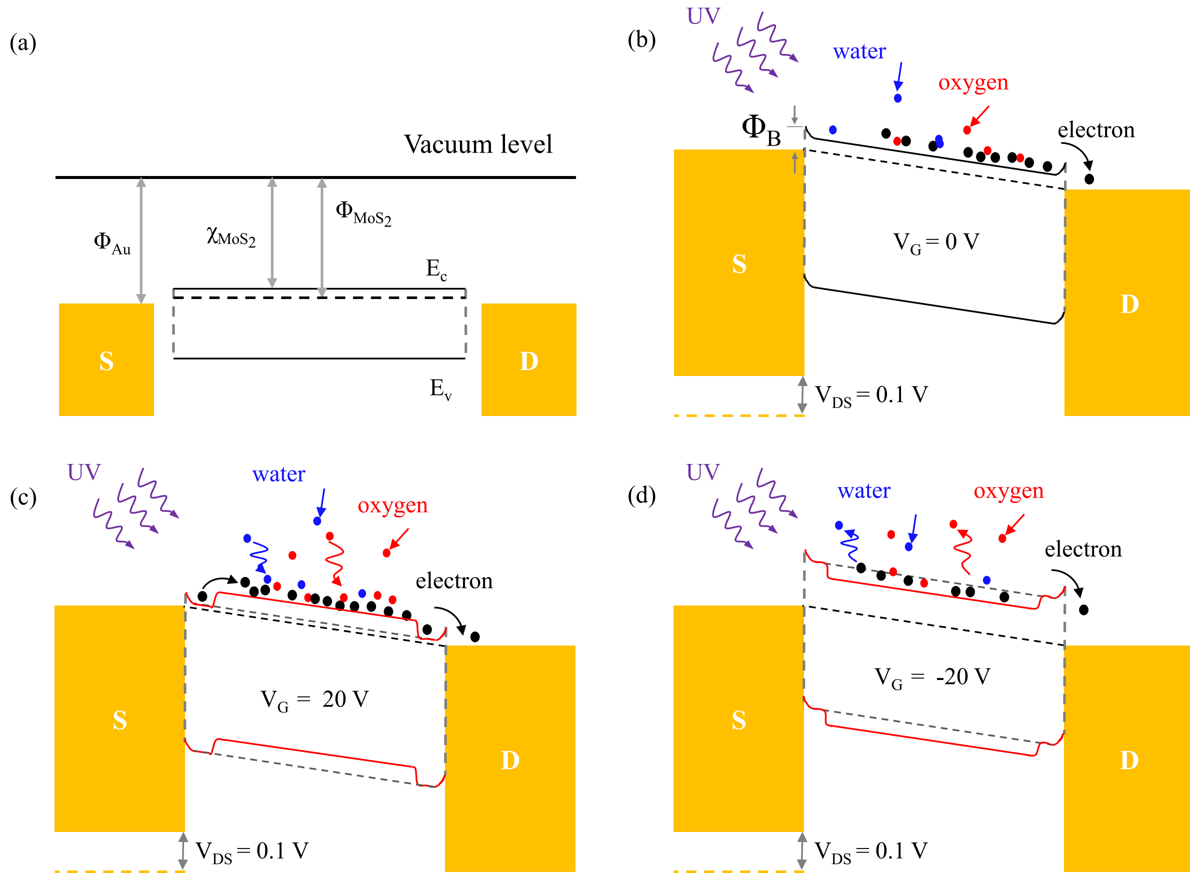

Figure 5. (a) Schematics of the energy level alignment of MoS_2 and source (S)–drain (D) electrodes. The energy band diagram at $V_{DS} = 0.1$ V in the ambient environment when (b) no gate-bias stress, (c) positive-gate-bias stress, and (d) negative-gate-bias stress was applied.

properties were different because of the gate-bias stress effect. The decay time constant τ_1 was observed to be slightly larger ($\tau_1 \sim 3.3 \times 10^4$ s) for a gate bias of -20 V (left plot of figure 4(a)) compared with the time constant for a zero gate bias ($\tau_1 \sim 2.8 \times 10^4$ s) (left plot of figure 4(b)) in vacuum. This result shows that the photocurrent for a -20 V gate bias decayed slower compared with the photocurrent for a zero gate bias. Additionally, we did not observe a value for τ_2 in the data from the left plot of figure 4(a) because we observed an increase in the current instead of a decay at the later stages. This current increase would be attributed to the release of the charges that were trapped at the interface trap sites by negative gate bias. These findings are consistent with our previous study that showed an increase in the current of MoS_2 FET devices with a negative-gate-bias stress because of a decrease in the charge trapping at oxygen sites on the MoS_2 surface [23]. In contrast, when we applied a gate bias of $+20$ V, we found a τ_1 of $\sim 6.5 \times 10^3$ and a τ_2 of $\sim 1.2 \times 10^6$ s (left plot of figure 4(c)), which were smaller than the values for zero gate-bias (left plot of figure 4(b)). This result shows that the photocurrent for a $+20$ V gate bias decayed faster compared with that for a zero gate bias. This finding was also consistent with our previous study that showed that the current of the MoS_2 FET device decreased with a positive-gate-bias stress because of the enhancement of charge trapping at oxygen sites on the MoS_2 surface [23]. In addition, the study showed that the oxygen adsorption on the MoS_2 surface is diminished (or enhanced) by the negative (or positive) gate bias [23].

The plots in the right panel of figure 4 display photoresponses of the device measured in oxygen environments. We observed a similar trend to the case measured in vacuum; the τ_1 was observed to be larger ($\tau_1 \sim 2.6 \times 10^3$ s) for a gate bias of -20 V (right plot of figure 4(a)) compared with that for a gate bias of 20 V ($\tau_1 \sim 1.6 \times 10^4$ s) (right plot of figure 4(c)) in an oxygen environment. When we applied a gate bias of $+20$ V, we found a τ_2 of $\sim 8.3 \times 10^3$ s (right plot of figure 4(c)), which was smaller than the τ_2 of $\sim 9.8 \times 10^3$ s for a gate bias of -20 V (right plot of figure 4(a)). Note that the decay time constant for zero gate bias (right plot of figure 4(b)) was smaller than that for a gate bias of 20 V (right plot of figure 4(c)) because the oxygen pressure for the right plot of figure 4(b) was larger than that for the right plot of figure 4(c). These results are consistent with our previous data in figure 3.

We now explain the observed photoresponses in terms of energy band diagrams. Figure 5 displays the schematics of the energy band diagrams of the MoS_2 channel between the source and drain electrodes. Figure 5(a) represents the energy level of each part of the MoS_2 FET. The tri-layer MoS_2 has a band gap energy of ~ 1.4 eV, a work function (Φ_{MoS2}) of 4.6–4.9 eV, and an electron affinity (χ_{MoS2}) of

~4.0 eV [22, 33–36]. We used Ti/Au as the source–drain electrodes that contact with the MoS_2. Because Ti was used as the adhesion layer for the Au electrodes, we considered the work function of Au (Φ_{Au}) (5.1–5.4 eV) for the band alignment with MoS_2. Therefore, the contact between Au and MoS_2 will have a very small Schottky barrier (Φ_B) as indicated in figure 5(b) [34]. Figure 5(b) shows the energy band diagram under UV illumination with applied biases $V_{DS} = 0.1$ V and $V_G = 0$ V (no gate-bias stress). UV light can generate electrons in the MoS_2 channel and photocurrent flow in the device as shown in figures 3 and 4, respectively. Figure 5(c) displays the band diagram under UV illumination with $V_{DS} = 0.1$ V and $V_G = 20$ V (the positive-gate-bias stress). Because of the positive-gate-bias stress, oxygen molecules can capture more electrons, thus creating more depletion in the MoS_2 channel. This phenomenon resulted in a faster decay of the photocurrent after the turn-off of the UV light with smaller decay time constants (figure 4(c)). Figure 5(d) displays the band diagram under UV illumination with $V_{DS} = 0.1$ V and $V_G = -20$ V (the negative-gate-bias stress). The negative-gate-bias stress causes electron accumulation in the MoS_2 channel. This phenomenon caused a slower decay of photocurrent after the turn-off of the UV light with a larger decay time constant (figure 4(a)).

4. Conclusion

In summary, we fabricated a multi-layer MoS_2 nanosheet FET and characterized the photoconductive properties using UV illumination under various environmental (vacuum or oxygen pressure) and measurement conditions. The photocurrent decay characteristics of the device after turn-off of the UV light were faster as the oxygen pressure increased. This result can be attributed to the charge trapping at the oxygen-related defect site on the MoS_2 surface. The photocurrent decay also depended on the gate-bias stresses. The photocurrent decay became slower (or faster) with negative (or positive) gate-bias stress compared with the case of zero gate bias. This phenomenon is due to the enhancement (or diminishment) of the charge trapping at oxygen sites on the MoS_2 surface. This study suggests that the environmental and electrical measurement conditions had a significant influence on the optoelectronic properties of the MoS_2 field-effect transistors.

Acknowledgments

The authors appreciate financial support by the National Creative Research Laboratory program (Grant No. 2012026372) and the National Core Research Center (Grant No. R15-2008-006-03002-0) provided by the National Research Foundation of Korea (NRF) grant, funded by the Korean Ministry of Science, ICT and Future Planning. S H acknowledges the support from the NRF grant (H-GUARD 2013M3A6B2078961).

References

[1] Novoselov K S, Geim A K, Morozov S V, Ziang D, Zhang Y, Dubonos S V, Grigorieva I V and Firsov A A 2004 *Science* **306** 666
[2] Radisavljivic B, Radenovic A, Brivio J, Giacometti V and Kis A 2011 *Nature Nanotechnol.* **6** 147
[3] Allen M J, Tung V C and Kaner R B 2010 *Chem. Rev.* **110** 132
[4] Wang X, Zhi L and Müllen K 2008 *Nano Lett.* **8** 323
[5] Xu Y, Bai H, Lu G, Li C and Shi G 2008 *J. Am. Chem. Soc.* **130** 5856
[6] Chen Z, Lin Y M, Rooks M J and Avouris P 2007 *Physica* E **40** 228
[7] Kam K K and Parkinson B A 1982 *J. Phys. Chem.* **86** 463
[8] Mak K F, Lee C, Hone J, Shan J and Heinz T F 2010 *Phys. Rev. Lett.* **105** 136805
[9] Bertolazzi S, Brivio J and Kis A 2011 *ACS Nano* **5** 9703
[10] Castellanos G A, Poot M, Steele G A, Zant H S and Agrait N 2012 *Adv. Mater.* **4** 772
[11] Eda G, Yamaguchi H, Voiry D, Fujita T, Chen M and Chhowalla M 2011 *Nano Lett.* **11** 5111
[12] Scalise E, Houssa M, Pourtois G, Afanas'ev V and Stesmans A *Nano Res.* **5** 43
[13] Perkins F K, Friedman A L, Cobas E, Campbell P M, Jernigan G G and Jonker B T 2013 *Nano Lett.* **13** 668
[14] Lee H S, Min S W, Park M K, Lee Y T, Jeon P J, Kim J H, Ryu S and Im S 2012 *Small* **8** 3111
[15] Wang H, Yu L, Lee Y H, Shi Y, Hsu A, Chin M L, Li L J, Dubey M, Kong J and Palacios T 2012 *Nano Lett.* **12** 4674
[16] Yin Z, Zeng Z, Liu J, He Q, Chen P and Zhang H 2013 *Small* **9** 727
[17] Radisavljevic B, Whitwick M B and Kis A 2011 *ACS Nano* **5** 9934
[18] Choi W, Cho M Y, Konar A, Lee J H, Cha G B, Hong S C, Kim S, Kim J, Jena D, Joo J and Kim S 2012 *Adv. Mater.* **24** 5832
[19] Li H, Yin Z, He Q, Li H, Huang X, Lu G, Fam D W H, Tok A I Y, Zhang Q and Zhang H 2012 *Small* **8** 63
[20] Kim S *et al* 2012 *Nature Commun.* **3** 1011
[21] Yin Z, Li H, Li H, Jiang L, Shi Y, Sun Y, Lu G, Zhang Q, Chen X and Zhang H 2011 *ACS Nano* **6** 74
[22] Lee H S, Min S W, Chang Y G, Park M K, Nam T, Kim H, Kim J H, Ryu S and Im S 2012 *Nano Lett.* **12** 3695
[23] Cho K, Park W, Park J, Jeong H, Jang J, Kim T Y, Hong W K, Hong S and Lee T 2013 *ACS Nano* **7** 7751
[24] Park W, Park J, Jang J, Lee H, Jeong H, Cho K, Hong S and Lee T 2013 *Nanotechnology* **24** 095202
[25] Davis S M and Carver J C 1984 *Appl. Surf. Sci.* **20** 193
[26] Late D J, Liu B, Matte H S S R, Dravid V P and Rao C N R 2012 *ACS Nano* **6** 5635
[27] Qiu H, Pan L, Yao Z, Li J, Shi Y and Wang X 2012 *Appl. Phys. Lett.* **100** 123104
[28] Studenikin S A and Cocivera M 2002 *J. Appl. Phys.* **91** 5060
[29] Jie J S, Zhang W J, Jiang Y, Meng X M, Li Y Q and Lee S T 2006 *Nano Lett.* **6** 1887
[30] Li Y, Valle F D, Simonnet M, Yamada I and Delaunay J J 2009 *Appl. Phys. Lett.* **94** 023110
[31] Li Q H, Gao T, Wang Y G and Wang T H 2005 *Appl. Phys. Lett.* **86** 123117
[32] Hao J, Studenikin S A and Cocivera M 2001 *J. Appl. Phys.* **90** 5064
[33] Han S W *et al* 2011 *Phys. Rev.* B **84** 045409
[34] Das S, Chen H Y, Penumatcha A V and Appenzeller J 2013 *Nano Lett.* **13** 100
[35] Liu K K *et al* 2012 *Nano Lett.* **12** 1538
[36] Giridharagopal R and Kelly K F 2008 *ACS Nano* **2** 1571